Solution Structures of Active and Inactive Forms of the DP IV (CD26) Inhibitor Pro-boroPro Determined by NMR Spectroscopy†

James L. Sudmeier,‡ Ulrich L. Günther,‡ William G. Gutheil,‡ Simon J. Coutts,§ Roger J. Snow,§ Randall W. Barton,§ and William W. Bachovchin*,‡

Department of Biochemistry, Tufts University School of Medicine, Boston, Massachusetts 02111, and Boehringer Ingelheim Pharmaceuticals, Inc., Ridgefield, Connecticut 06877

Received April 11, 1994; Revised Manuscript Received July 20, 1994®

ABSTRACT: Synthesis of the boronic acid analog of the dipeptide Pro-Pro yields a mixture of diastereomers Pro-L-boroPro and Pro-D-boroPro, one of which is a potent inhibitor [K_i = 16 pM; Gutheil, W. G., & Bachovchin, W. W. (1993) *Biochemistry 32,* 8723–8731] of dipeptidyl amino peptidase type IV (DP IV), also known as CD26. The structures of both diastereomers are determined here in aqueous solution by means of 1D and 2D NMR of ^1H, ^{13}C, and ^{11}B, and force-field calculations, and the inhibitor is proven to have the L–L configuration. At low pH values (~2), both diastereomers are *trans* with respect to the peptide bond. Populations of proline ring conformers are determined by pseudorotation analysis, using vicinal proton spin-coupling constants obtained by computer analysis of 1D ^1H NMR spectral fine structure. At neutral pH values, the Pro-boroPro inhibitor of DP IV undergoes slow, reversible inactivation (Gutheil & Bachovchin, 1993). By structural determination of the decomposition products of both diastereomers, the process is shown here to involve formation of a six-membered ring between the residues by means of *trans–cis* conversion and formation of a B–N bond, producing chiral nitrogen atoms in both cases having the *S* configuration. Analogy to cyclic dipeptides suggests the new compounds be named *cyclo*(Pro-L-boroPro) and *cyclo*(Pro-D-boroPro).

Dipeptidyl amino peptidase type IV (DP IV),[1] also known as CD26, is a membrane-anchored, highly glycosylated dimer (molecular mass 110 kDa per subunit) which occurs widely in mammalian cells and tissues and exhibits specific exoprotease activity for terminal Xaa-Pro dipeptides. A number of biological functions of DP IV have been proposed, including amino acid salvage (Miyamoto et al., 1988, 1987), fibronectin-mediated cells movement and adhesion (Hanski et al., 1988, 1985), processing of peptides, e.g., growth hormone releasing factor (Frohman et al., 1989), and T cell activation and immune system regulation (Ansorge & Schön, 1987; Schön et al., 1989, 1987, 1985). Among hematopoietic cells, DP IV is found mainly on CD4+ T helper cells, and surface expression increases markedly upon their activation (Schön & Ansorge, 1990). DP IV-positive cells include those responsible for recall antigen responses (Hafler et al., 1989, 1986). Inhibitors of DP IV suppress antigen-induced T cell proliferation in cell cultures (Flentke et al., 1991) and suppress antibody production in vivo in mice (Kubota et al., 1992). Recently, DP IV (CD26) was reported to be essential for entry of the HIV-1 virus in CD4+ T cells (Callebaut et al., 1993). On the basis of the observation of decreased viral entry in the presence of DP IV inhibitors, these workers propose that DP IV catalytic activity is essential to the process.

Pro-boroPro is a member of a class of extraordinarily potent serine protease inhibitors known as "peptide boronic acids", whose high affinities for their target enzymes are attributed in large part to close mimicry by boronyl–serine adducts of tetrahedral transition states in enzyme-catalyzed reactions. Of several known Xaa-boroPro inhibitors of DP IV, Pro-boroPro is thus far the best characterized, having a K_i value of 16 pM (Gutheil & Bachovchin, 1993). Furthermore, the Pro–Pro bond is not subject to proteolytic cleavage by any known enzyme. Such unusual inhibitory potency and degradation resistance make Pro-boroPro very promising as a therapeutic agent for immune system modulation, and if the proposal of Callebaut et al. proves correct, for blocking cellular entry of the HIV virus in AIDS patients.

The synthesis of Pro-boroPro (Bachovchin et al., 1990) produces racemic boroPro, which is coupled with L-proline to produce a mixture of L,L and L,D diastereomers (structures I and II).

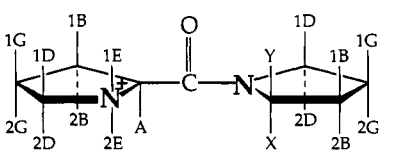

I : Pro-L-boroPro; X = A; Y = $B(OH)_2$

II : Pro-D-boroPro; Y = A; X = $B(OH)_2$

After separation by HPLC, one of the diastereomers proved to be a better inhibitor of DP IV by orders of magnitude, but

† Supported by Research Grant AI 31866 from the National Institutes of Health.

* Author to whom correspondence should be addressed.

‡ Tufts University School of Medicine.

§ Boehringer Ingelheim Pharmaceuticals, Inc.

® Abstract published in *Advance ACS Abstracts,* September 15, 1994.

[1] Abbreviations: DP IV, dipeptidyl amino peptidase type IV; CD26, cluster of differentiation 26; COSY, 2D correlation spectroscopy; 2QF-COSY, 2 quantum-filtered COSY; TOCSY, 2D total correlation spectroscopy; NOESY, 2D nuclear Overhauser effect spectroscopy; FID, free-induction decay; D_2O, deuterium oxide. The prefix "boro" indicates that carboxylate groups of amino acid residues are replaced by -$B(OH)_2$. Protons are labeled according to the Protein Data Bank convention, except for pseudorotation analyses, where Altona's convention is used (Altona, 1992).

0006-2960/94/0433-12427$04.50/0

its stereochemical identity was unknown (Gutheil & Bachovchin, 1993), although the absolute configuration of one enantiomer of boroPro has been determined (Kelly et al., 1993a). Other questions arose concerning the nature of the inactivation products which formed reversibly at neutral pH values. Therefore a comprehensive study of the solution structure of Pro-boroPro and its inactivation products was undertaken.

Although Pro-boroPro is relatively small, determination of its true structure in solution is far from simple. In the present study, the identities and conformational populations of both diastereomers and their inactivation products are determined. Our strategy employs multinuclear and 2D NMR but also relies heavily upon ^{1}H 1D fine structure analysis, which is only marginally feasible owing to strong overlap of dual seven-spin systems. The NMR spectral analysis and computational methods employed here should prove applicable to other small, conformationally labile compounds, and the results should assist in future studies of both free and enzyme-bound boronic acid inhibitors.

MATERIALS AND METHODS

Preparation of Pro-L-boroPro and Pro-D-boroPro NMR Samples. Pro-boroPro was synthesized as described previously (Bachovchin et al., 1990) and purified by C18 HPLC (Gutheil & Bachovchin, 1993). The eluates were subsequently lyophilized and dissolved in either deionized water or 99.9% D_2O. Sample pH values were adjusted by addition of 6 M stock solutions of either HCl, NaOH, deuterium chloride (DCl), or sodium deuteroxide (NaOD). As long as 8 h were allowed for attainment of pH equilibrium. Sample concentrations were typically ~6 mM. The concentration of the more abundant L–D isomer, however, was ~20 mM for the ^{13}C studies. Although a solvent may be referred to as "H_2O" for brevity, all samples contained a minimum of 10% D_2O for the NMR spectrometer field/frequency lock. Prior to NOESY experiments, all samples were deoxygenated by gently bubbling with nitrogen or argon gas for about a minute.

NMR Spectrometers. With one exception (see Acknowledgments) the NMR experiments were carried out on the Tufts Bruker AMX-500 and Bruker AM-400 spectrometers. The AMX-500 is equipped with an X-32 computer (CPU 3), multichannel interface, and a 5-mm triple-resonance probe. A 10-mm broad-band probe, the ^{11}B background of which was reduced by substitution of quartz for all Pyrex Dewars and inserts, was also employed on the AMX-500. The AM-400 is equipped with a wide-bore magnet, Aspect 3000 computer, digital phase shifters, and a variety of probes, including a 10-mm ^{13}C probe.

NMR Experiments. For all ^{1}H spectra the carrier frequency was centered on the solvent peak, which also served as spectral reference (4.760 ppm at 298.3 K and 4.960 ppm at 278.3 K). For ^{1}H spectra in D_2O a sweep width of 8 ppm was generally used, but for samples in H_2O, greater sweep widths (11 ppm) were required for inclusion of the low-field N–H resonances. To increase the ^{1}H 1D spectral resolution, samples were spun, 32K total data points were acquired, and Lorentzian–Gaussian apodization (Ferrige & Lindon, 1978) using LB = –1.5 Hz and GB = 0.3 with one zero-fill were employed before Fourier transformation. All spectral processing was carried out using standard Bruker software, UXNMR and DISNMR. Solvent suppression using soft-pulse presaturation (Campbell et al., 1974) with a relaxation delay of 1.3 s and attenuation HL2 of 55–58 dB was normally employed during ^{1}H spectral acquisition, except for experiments employing "jump–return" nonexcitation of H_2O (Clore et al., 1983) in order to avoid saturation transfer of -NH resonances. Most 2D ^{1}H experiments were carried out on our Bruker AMX 500 using the 5-mm triple-resonance probe. The 90° hard pulses with 1 dB attenuation (HL1 = 1) ranged from 7.4 to 8.1 μs. These experiments involved the acquisition of 512 FIDS, each consisting of 2 K total data points. With one zero-fill in the f_1 dimension, sizes of the full transformed matrices were f_2 =1K by f_1 = 512 complex data points. All 2D spectra were run in the phase-sensitive mode using TPPI [time-proportional phase incrementation (Marion & Wuthrich, 1983)]. Reduction in the residual solvent was achieved by the "QPOL" command in UXNMR, which baseline corrects each FID by subtracting an empirically fit polynomial prior to Fourier transformation. After transformation in both dimensions and phase correction, all spectra were baseline corrected using "ABS2".

2QF-COSY spectra (Rance et al., 1983) were recorded using a 16-step phase cycle designed for reduction of rapid-pulsing artifacts (Derome, 1990). TOCSY spectra (Braunschweiler & Ernst, 1983) were recorded using a mixing time of 72 ms and a "clean" DIPSI-2 (Shaka et al., 1988) mixing sequence designed for reduction of cross-relaxation effects (Cavanagh & Rance, 1992) with 13 dB attenuation and equal (30 μs) on and off times. Lorentzian–Gaussian window functions were generally used in the f_2 dimension and either Lorentzian–Gaussian or shifted sine bell in the f_1 dimension. For the NOESY experiments (Kumar et al., 1980) with solvent presaturation or "jump–return", we employed a pulse program with an extended 64-step phase cycle for artifact reduction and a mixing time of 600 ms. NOESY spectra were processed using Lorentzian–Gaussian window functions in both dimensions with LB2 = –8 Hz, GB2 = 0.05, LB1 = –8 Hz, and GB1 = 0.10.

^{11}B spectra were carried out using 5-mm samples in the Bruker AMX 500 10-mm broad-band probe. Using a sweep width of 20 000 Hz, 8K total data, and a relaxation delay of 0.3 s, we obtained sufficient signal to noise within 30–60 min. All ^{11}B spectra were referenced vs boric acid at δ = 0.0 ppm. A broad hump arising partly from materials inside the probe and partly from the natural quartz NMR tubes employed was reduced by convolution difference (Campbell et al., 1973) in the frequency domain using values of line broadening LB = 1000 Hz and 100 Hz.

Computations. Analysis of ^{1}H 1D fine structure was carried out using the FORTRAN program LAOCN5 (Attimonelli & Sciacovelli, 1980), an expanded and improved version of LAOCOON 3 (Bothner-by & Castellano, 1968). LAOCN5 was obtained from the Quantum Chemistry Program Exchange (Indiana University, QCPE No. 458) and adapted for SUN Microsystems Sparc II and Apollo/HP DN3500 workstations. A Lorentzian line shape routine, high-resolution screen plot, spectral editing dialogue, and grid parameter search was added to the Apollo version to facilitate initial trials. Pseudorotation analysis was carried out using the FORTRAN program PSEUROT 5.4 (De Leeuw & Altona, 1983; Altona, 1992), which was adapted for the Sparc II and Apollo workstations. Force-field calculations were carried out using CHARMm 22 (Brooks et al., 1983; Momany & Rone, 1992) and QUANTA 3.3 (Molecular Simulations, Inc., Burlington, MA) on a Silicon Graphics 4D70GT workstation. Molecular coordinates were exported from QUANTA and sent over the local network for additional processing on the Apollo, as were NOESY cross-peak integration files from the Bruker AMX500.

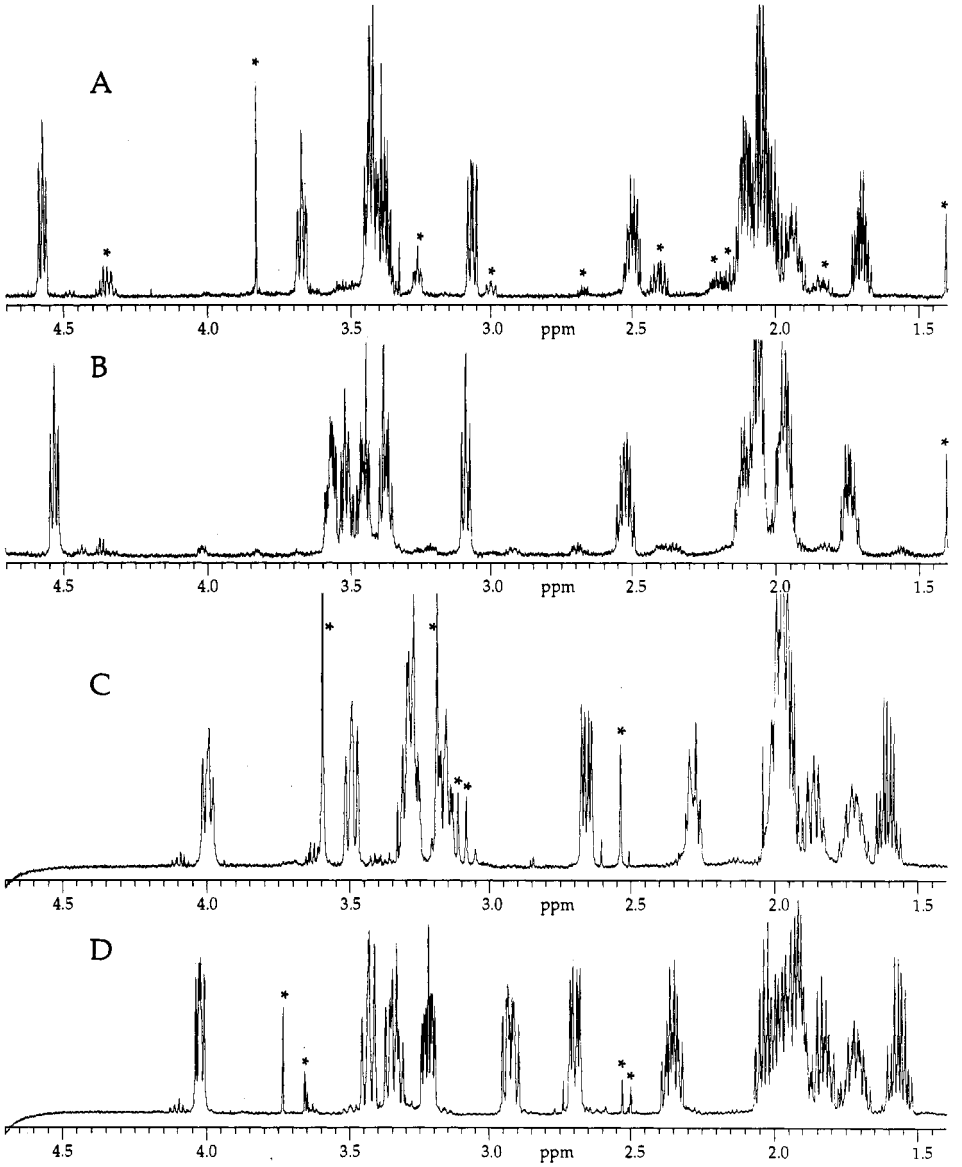

FIGURE 1: 1D ^{1}H NMR spectra in D_2O at 25 °C. (A) Compound I, pH 2, 600 MHz; (B) II, pH 2, 600 MHz; (C) III, pH 7, 500 MHz; (D) IV, pH 7, 500 MHz. Asterisks denote sample impurities. The tops of the highest peaks in A, B, and C are clipped for compactness.

RESULTS AND DISCUSSION

NMR Spectral Assignment and Compound Identification. 1D ^{1}H NMR spectra of compounds I and II (pH 2) are shown in Figure 1, spectra A and B, and spectra of their corresponding decomposition products (pH 7) are shown in Figure 1, spectra C and D. To determine unambiguously by NMR that Figure 1A represents compound I and Figure 1B represents II, rather than vice versa, and to determine the identities of their respective decomposition products, stereospecific assignment of all proton resonances of the four compounds was undertaken.

Some facts are evident by inspection of the α hydrogen resonances alone (Van Wijk et al., 1992). Because of the tendency of the boronic acid group to cause strong (~1.5 ppm) upfield shifts of neighboring geminal protons, the lowest field resonances in Figure 1A–D are assigned to α hydrogen atoms of the N-terminal proline residues, while the boroPro ring α hydrogen atoms are found near 3.1 ppm at pH 2 (Figure 1A,B) and near 2.7 ppm at pH 7 (Figure 1C,D). Spin-coupling of the α hydrogen atoms to neighboring β hydrogens may produce either four-line multiplets (e.g., Figure 1A at 3.1 ppm), indicating two dissimilar vicinal coupling constants, or triplets (e.g., Figure 1B at 3.1 ppm), indicating similar coupling constants. The triplet shows averaging between comparable amounts of two or more conformers, whereas the four-line pattern indicates strong preference for a single conformer. The presence of several α hydrogen triplets in Figure 1 indicates that significant conformational averaging does occur.

Complete assignment of all proton resonances in Figure 1 was complicated by numerous peak overlaps and the presence of impurities (marked with asterisks), including a slowly growing decomposition product suspected of arising from air-oxidative cleavage of the alkyl boronic acid [boron(I)] to boric acid [boron(III)]. Chemical shift degeneracy of gamma hydrogen atoms and some β and δ hydrogens was sometimes virtually complete (within .001 ppm). With the aid of 2D NMR and computer analysis of the 1D ^{1}H NMR spectral fine structure at various frequencies, complete assignment of the ^{1}H NMR spectra of the four compounds was achieved.

500-MHz 2D ^{1}H spectra (COSY, TOCSY, and NOESY) of I, II, and their decomposition products were collected. Typical results for I are shown in Figure 2. The COSY spectrum in Figure 2A reveals pairwise proton correlations

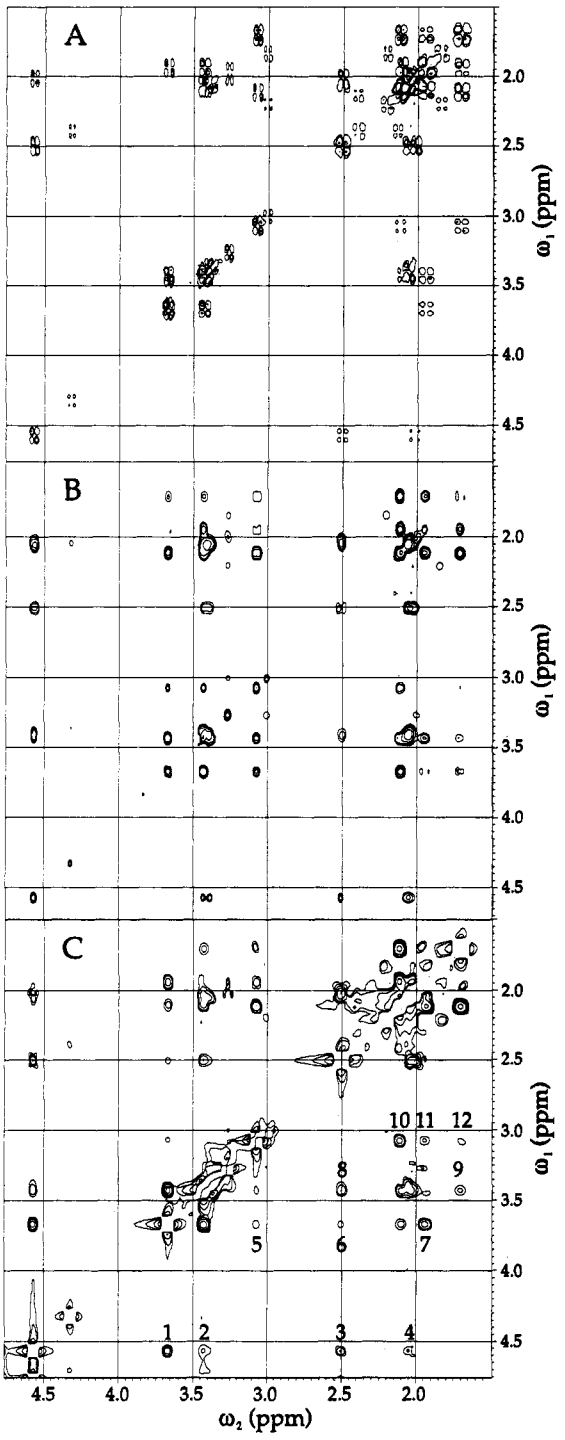

FIGURE 2: 2D ^{1}H 500-MHz spectra of compound I, pH 2, in D_2O at 25 °C. (A) 2QF-COSY; (B) TOCSY, mixing time = 72 ms; (C) NOESY, mixing time = 600 ms.

through two or three bonds. The TOCSY spectrum (Figure 2B) exhibits proton connectivities through two to four bonds, aligning all cross-peaks of each proline spin system in rows and columns. NOESY spectra (e.g., Figure 2C) reveal ^{1}H connectivities through space, including any interresidue contacts.

As was the case for the 1D ^{1}H spectra, chemical shift degeneracy confounded the interpretation of the 2D ^{1}H NMR spectra, resulting in substantial cross-peak overlap, especially in the TOCSY and NOESY spectra. Nevertheless, the combined 1D and 2D assignment strategy permits at least 12 cross-peaks in the NOESY spectrum (Figure 2C) to be assigned unambiguously to I. The cross-peak labels in Figure

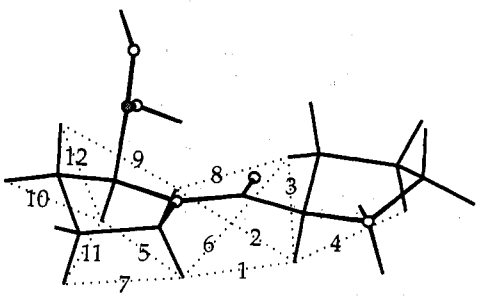

FIGURE 3: Conformer of compound I, showing some through-space interactions assigned by NMR. The numbering corresponds to NOESY cross-peaks in Figure 2C.

2C correspond to the dotted lines showing ^{1}H–^{1}H interactions in the structure of I in Figure 3. The web of through-space proton interactions determines the stereospecific assignments of all geminal proton pairs on the boroPro ring, the L configuration of the boroPro ring, and the *trans* orientation of the peptide bond, enabling the strong interaction of boroPro δ hydrogen atoms with Pro α and β hydrogens (cross-peaks 1, 2, 6, and 8 in Figure 2C and dotted lines in Figure 3). Stereospecific assignment of the δ hydrogen atoms is the key to determining the identities of diastereomers I and II. For the boroPro ring of I, for example, the β hydrogens can be identified by the large (11.2 Hz) *trans* A–1B spin-coupling constant. Likewise the γ and δ geminal pairs can be assigned due to large 1B–2G and 2G–1D spin-couplings (11.0 and 10.1 Hz respectively). However, due to strong overlap of the δ hydrogens and the overlapping β and γ hydrogens, the 1D spectral analysis may not have been possible without NOESY cross-peaks such as 5, 9, and 11 (Figure 2C) relating protons on the same side of the ring.

Computer analysis of the 1D ^{1}H NMR fine structure was achieved for all eight seven-spin proline cases of the four compounds, an example of which is shown in Figure 4. The observed 600-MHz spectrum of I, the upfield portion of which is shown in Figure 4A,was simulated, despite the interference of chemical shift degeneracy and impurities, as shown in Figure 4D, which is a summation of the boroPro (Figure 4B) and Pro (Figure 4C) subspectra.

Good agreement between simulated and observed spectra such as those in Figure 4E,F and the corresponding 400-MHz spectra yields the assignments in Table 1. As shown in earlier computer analyses of proline ^{1}H NMR fine structure (Pogliani et al., 1975), even highly degenerate proton chemical shifts, such as those of typical γ and β hydrogen atoms, can be determined accurately by their strong influence on remote multiplets, such as those of neighboring α hydrogens. 1D computer analyses, as well as aiding in the assignment process, provide vicinal proton spin-coupling constants, which yield valuable information regarding the structure and abundance of various conformers.

Accuracy of the parameters in Table 1 is estimated at ±0.4 Hz, although in some cases, because of chemical shift degeneracy, greater line widths, and/or impurities, it may be 1–2 Hz. Overall accuracy of the spectral analyses was limited by rather large ^{1}H NMR line widths (typically 1.2–1.5 Hz). In some cases, the fit was improved by introduction of four-bond spin-coupling constants ($\leq|0.8|$ Hz) along "W" coupling paths. The effect of four-bond couplings along nonplanar paths [generally $\leq|-0.4|$ Hz (Pogliani et al., 1975)] was not explored in these simulations.

Table 1 also includes chemical shifts of the exchangeable low-field -N-H protons on Pro (2E and 1E), which are observable in H_2O solvent. There are two broad (~50 Hz)

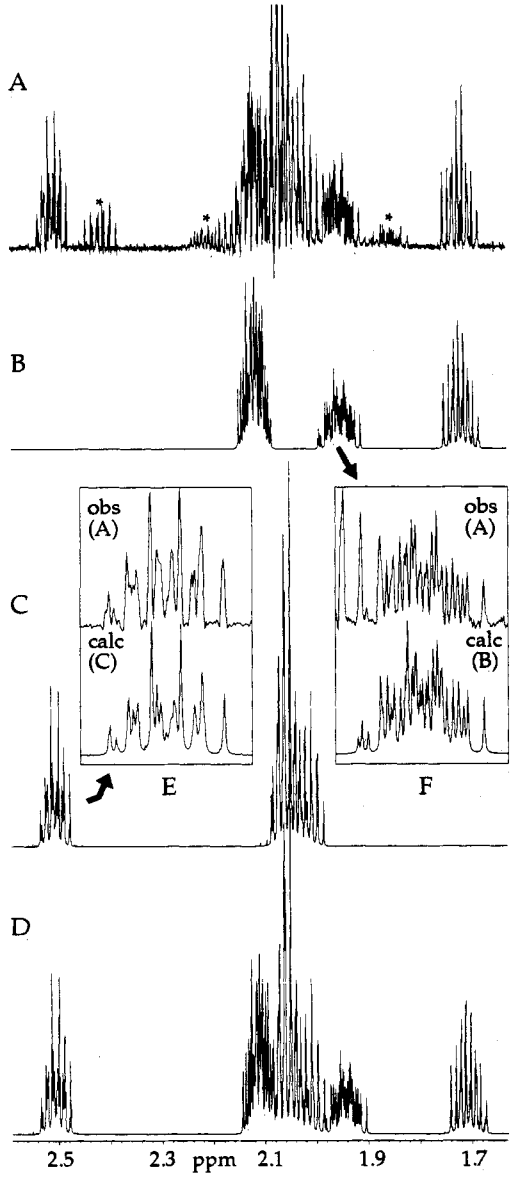

FIGURE 4: Example of fine structure analysis of 1D ^{1}H NMR spectra. (A) Observed partial 600-MHz spectrum of compound I, expanded and resolution-enhanced version of Figure 1A. (B) Computer simulation of A arising from boroPro ring. (C) Same as B arising from Pro ring. (D) Summation of computer simulated subspectra B and C. (E) Expansion of multiplet at 2.5 ppm, showing fit of calculated and observed spectra. (F) Same as E for multiplet at 1.94 ppm.

low-field resonances for I and II in H_2O and new spin-couplings in the α and δ multiplets of Pro. Assignment of 2E and 1E is based on NOESY spectra in H_2O showing a cross-peak between 2E and A of Pro. Cross-peaks between 2E and 2D and between 1E and 1D reinforce all four assignments. Because of rapid exchange even at 5 °C, the low-field -N-H resonances of I and II are observable only by techniques for avoiding H_2O excitation, such as "jump–return" (Clore et al., 1983), rather than H_2O presaturation (Campbell et al., 1974), which leads to disappearance of the -N-H resonances through saturation transfer.

The decomposition products of I and II at pH 7, however, show only a single low-field -N-H resonance (Table 1), both of which are assigned to 2E on the basis of NOESY spectra in H_2O showing through-space connectivities to A and 2D of Pro. The decomposition product of I also exhibits a strong cross-peak between 2E of Pro and A of boroPro, providing unequivocal evidence of a *cis* peptide bond. The ^{11}B NMR spectrum of the decomposition product of I as shown in Table 2 exhibits a single resonance at −17.6 ppm upfield of boric acid, which is characteristic of tetrahedral boron atoms (Kidd, 1983; Tsilikounas et al., 1993). These observations confirm earlier speculation regarding formation during the slow, reversible decomposition of I of a boron–nitrogen bond (Flentke et al., 1991; Gutheil & Bachovchin, 1993; Kelly et al., 1993b), like the B–N bond in a recent X-ray crystallographic structure of the Pro-L-boroPro pinenediol decomposition product (Snow et al., unpublished data), proving the existence of structure III, a new boronic acid analog of *cyclo*(Pro)$_2$ (Putochin, 1926).

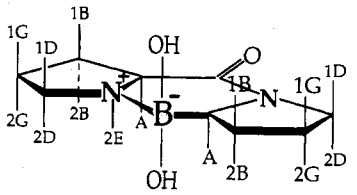

III: *cyclo* (Pro-L-boroPro)

The decomposition product of II is also proven to contain a tetrahedral boron atom as shown by the chemical shift (−17.1 ppm) of its ^{11}B resonance in Table 2. The ^{1}H NOESY spectrum of the decomposition product of II in H_2O exhibits no interresidue cross-peaks, which is consistent with the *cis* conformer and boron–nitrogen bond (structure IV), taking

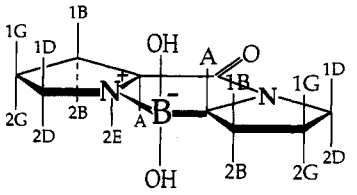

IV: *cyclo* (Pro-D-boroPro)

into account the larger interresidue proton distances in *cyclo*(Pro-D-boroPro). The nitrogen atoms involved in B–N bond formation possess the *S* configuration in both compounds III and IV.

Low-field -N-H protons in *cyclo*(Pro-L-boroPro) (III) and *cyclo*(Pro-D-boroPro) (IV) are shifted upfield compared to the -N-H protons in I and II as shown in Table 1 and are considerably narrower, nearly sufficient to resolve the quartets caused by spin-coupling of neighboring protons A, 2D, and 2E. Line-narrowing is caused by longer -N-H proton lifetimes for III and IV, as demonstrated by their observation (partially in the case of III, and fully in the case of IV) during presaturation of H_2O, even at 25 °C.

^{11}B NMR spectra of I and II exhibit multiple resonances, as shown in Table 2. Two ^{11}B resonances downfield of boric acid indicate different types of trigonal boron atoms in slow exchange, possibly diborate species linked by -B-O-B- bonds, which would also help explain the rather large ^{1}H line widths. The ^{11}B NMR spectrum of I also reveals about 10% of cyclic product III at pH 2, showing an effective pK_a value of about 3. The ^{11}B spectrum of II contains about 30% additional cyclic product IV at pH 2, showing an effective pK_a value of about 2.5. Greater depression of proline's pK_a value by IV indicates greater stability of IV vs III. A few percent of free boric acid also appears in the ^{11}B spectra of I and II, probably caused by slow, oxidative cleavage.

Table 1: Proton Chemical Shifts, δ (ppm), and Spin-Coupling Constants, J (Hz)

	boroPro							Pro								
	A	2B	1B	2G	1G	2D	1D	A	2B	1B	2G	1G	2D	1D	2E	1E
Pro-L-boroPro																
δ	3.074	2.119	1.708	1.944	2.105	3.674	3.430	4.571	2.505	2.016	2.056	2.066	3.385	3.432	8.96	8.16
J(A–)		6.9	11.2	0.0	0.0	0.0	0.0		8.5	7.2	0.0	0.0	0.0	0.0	~4–7	~4–7
J(2B–)			–12.3	6.6	3.2	0.0	0.0			–13.5	5.7	7.7	0.0	0.0	0.0	0.0
J(1B–)				11.0	6.1	0.0	0.0				7.6	7.2	0.0	0.0	0.0	0.0
J(2G–)					–12.4	8.2	10.1					–12.9	6.5	~8	0.0	0.0
J(1G–)						2.8	7.1						7.6	~7	0.0	0.0
J(2D–)							–10.4							–11.6	~4–7	~4–7
J(1D–)															~4–7	~4–7
Pro-D-boroPro																
δ	3.088	1.742	2.118	2.061	1.975	3.512	3.563	4.527	2.523	1.961	2.060	2.061	3.373	3.452	8.96	8.19
J(A–)		9.4	8.1	0.0	0.0	0.0	0.0		8.7	7.4	0.0	0.0	0.0	0.0	~4–7	~4–7
J(2B–)			–12.6	6.5	9.4	0.0	0.0			–13.5	5.6	7.9	0.0	0.0	0.0	0.0
J(1B–)				4.6	6.6	0.0	0.0				~8	~7	0.0	0.0	0.0	0.0
J(2G–)					–12.4	8.7	3.8					~–13	9.5	6.5	0.0	0.0
J(1G–)						7.2	8.0						4.9	7.7	0.0	0.0
J(2D–)							–10.2							–11.4	~4–7	~4–7
J(1D–)															~4–7	~4–7
cyclo(Pro-L-boroPro)																
δ	2.662	1.958	1.610	1.728	1.982	3.494	3.284	3.997	2.289	1.962	1.863	2.007	3.161	3.287	6.427	
J(A–)		5.9	12.3	0.0	0.0	0.0	0.0		7.5	11.2	0.0	0.0	0.0	0.0	~7	
J(2B–)			–12.5	6.7	~0	0.8	0.0			–12.6	7.6	2.1	0.0	0.0	0.0	
J(1B–)				12.3	6.6	0.0	0.0				10.7	8.0	0.0	0.0	0.0	
J(2G–)					–12.3	9.3	11.1					–12.6	9.3	9.2	0.0	
J(1G–)						1.0	7.0						3.5	7.8	0.0	
J(2D–)							–12.0							–11.6	~7	
J(1D–)															~7	
cyclo(Pro-D-boroPro)																
δ	2.700	1.569	1.933	1.973	1.720	3.342	3.430	4.022	2.358	2.034	1.829	1.915	3.220	2.929	6.313	
J(A–)		12.3	6.2	0.0	0.0	0.0	0.0		5.5	8.2	0.0	0.0	0.0	0.0	~7	
J(2B–)			–12.2	6.3	12.4	0.0	0.0			–13.4	8.1	8.5	0.0	0.0	0.0	
J(1B–)				0.6	6.6	0.0	0.0				7.9	5.7	0.0	0.0	0.0	
J(2G–)					–12.4	7.0	0.6					–13.0	7.2	9.3	0.0	
J(1G–)						11.0	9.5						4.2	7.1	0.0	
J(2D–)							–11.9							–11.7	~7	
J(1D–)															~7	

Table 2: ^{11}B NMR Parameters

compound	chemical shifts δ (ppm)[a]	line widths (Hz)
Pro-L-boroPro	8.8 (60%), 10.9 (40%)	~200, ~500
Pro-D-boroPro	9.7 (30%), 10.6 (70%)	~200, ~500
cyclo(Pro-L-boroPro)	–17.6	~150
cyclo(Pro-D-boroPro)	–17.1	~150

[a] Chemical shift relative to boric acid at δ = 0.0 ppm.

In the early stage of spectral assignment, valuable information was obtained by the use of a ^{1}H/^{13}C 2D NMR correlation experiment "heteronuclear DEPT" (Bendall & Pegg, 1983), involving direct observation of natural abundance ^{13}C. This experiment was possible only for the more plentiful samples, but enabled the correlation of all geminal ^{1}H pairs. ^{13}C chemical shifts and ^{13}C–^{1}H spin coupling constants are reported in Table 3.

Pseudorotation Analysis. Instability of a planar arrangement of atoms in saturated five-membered rings is caused by unfavorable internal and torsion angles (Eliel et al., 1965). Such rings are puckered by displacement of one atom ("envelope") or two atoms ("twist") as shown in Figure 5. The infinite variety of such conformers has been systematized by *pseudorotation* theory, where each conformer represents a single point in a polar coordinate system, described by two parameters: a maximum pucker angle, Φ_m, and a phase angle, P (Altona & Sundaralingam, 1972). For heterocycles such as D-ribose or L-proline, zero phase angle is defined as the twist conformer in which C3 (C3′ or Cγ) is above the C1–X–C4 plane and C2 (C2′ or Cβ) is below the plane viewed as shown in Figure 5 (where N is remote from the viewer and C1 (C1′ or Cα) is on the right-hand side). From this reference point, there is a 360° wheel of additional twist conformers,

Table 3: ^{13}C Chemical Shifts, δ (ppm), and ^{13}C–^{1}H Spin-Coupling Constants, ^1J (Hz)

	boroPro				Pro				
	CA	CB	CG	CD	CA	CB	CG	CD	C
Pro-L-boroPro									
δ	49.2[a]	27.4	27.4	47.9	59.8	28.9	24.7	47.3	167.3
Pro-D-boroPro									
δ	49.0[a]	27.4	27.1	47.8	59.5	29	24.7	47.4	167.3
^1J	~132	135	128	143	150	136	135	147	
cyclo(Pro-L-boroPro)									
δ		27.5	~23	47	61.5	28.4	~24	44.5	
cyclo(Pro-D-boroPro)									
δ		27.2	23.6	47.3	60.3	30.5	23.6	47.7	168.4

[a] Broadened by directly attached boron atom.

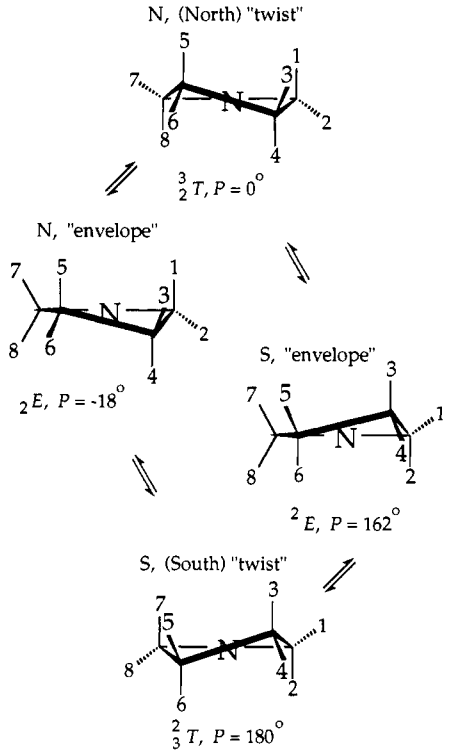

FIGURE 5: Schematic diagram of pseudoration "phase wheel". The structures shown are representative of 20 benchmark "twist" and "envelope" conformers and an infinity of intermediate structures. The numbering of substituents 1–8 is utilized in all pseudoration analyses, regardless of optical isomer. Carbon 1 (C1′ or Cα) is on the right-hand side and carbon 4 (C4′ or Cδ) on the left.

envelopes, asymmetric twists, etc., some of which are depicted in Figure 5. The top half of the phase wheel ($-90^\circ < P < 90^\circ$) represents confomers labeled "N" (north), while the bottom half of the wheel ($90^\circ < P < 270^\circ$) represents "S" (south) conformers.

Given the puckering amplitude, Φ_m, and orientation, P, for a symmetrical ring one can easily calculate θ_0–θ_4, the five endocyclic angles, i.e., torsion angles involving ring atoms, beginning at C1–C2–C3–C4. By means of the equation

$$\theta_j = \Phi_m \cos (P + 0.8\pi j) \quad (1)$$

where j = 0–4, ring geometry is completely defined. The original definition of "N" and "S" confomers (Altona & Sundaralingam, 1972) was based on the sign of θ_0 being positive for "N" conformers and negative for "S" conformers regardless of the chirality of C1. Thus we apply these definitions to L-Pro and D-Pro alike, even though historical definitions of *exo* and *endo* may be violated in the process (De Leeuw et al., 1983a).

Determination of the proline ring conformations in structures I–IV goes beyond the values of $^3J_{HH}$, the average vicinal ^{1}H spin-coupling constants in Table 1. It also requires knowledge of the relationships between $^3J_{HH}$ and ϕ_{HH}, the proton torsion angle, and between ϕ_{HH} and pseudorotational parameters Φ_m and P, taking into account any distortion of ring atoms from tetrahedral. These relationships are integral to the computer program PSEUROT 5.4 (Altona, 1992), which fits $^3J_{HH}$ to the optimal binary mixture of conformers, yielding fractional populations, X, which determine $^3J_{av}$, the weighted averaged spin-coupling constant

$$^3J_{av} = X_N {}^3J_N + X_S {}^3J_S \quad (2)$$

Table 4: Group Electronegativities, λ, for ProboroPro in D_2O

group	compound	^3J (Hz)	λ	reference
-NHR	diethylamine	7.08	1.29	this work
$-NH_2R^+$	diethylamine HCl	7.18	1.12[a]	this work
-NR(COR′)	*N*,*N*′-diethylacetamide (both ethyl groups)	7.18	1.12[a]	this work
$-NHB(OH)_2R$	1:1 diethylamine methylboronate	7.26	0.98	this work
$-B(OH)_2$			0.05[b]	this work
-COOH(or R)			0.42	Altona (1992)
-C			0.65	Altona (1992)

[a] Calculated from formula $\lambda = (7.84 - J)/0.59$ (Altona et al., 1989). [b] Obtained from best fit to data presented in this work.

and the pucker angles, Φ_m, and phase angles, P, of both species. The relationship between proton torsion angles and pseudorotation parameters is given by

$$\theta_{HH} = B + A\Phi_m \cos (P + \text{phase}) \quad (3)$$

where constants A, B, and phase are obtained by empirical fitting of X-ray crystallographic structures, in conjunction with neutron diffraction studies (Haasnoot et al., 1981). Because of the relatively small amount of such data available for prolines, the constant A is set equal to unity, and phase is not allowed to deviate from -0.8π (−144°, C1–C2 torsions), 0° (C2–C3), or 0.8π (144°, C3–C4). The values employed for constant B, reflecting deviations from ideal 120° projection symmetry for each torsional pair are as follows: 1–3, −1.7°; 1–4, −122.9°; 2–3, 122.9°; 2–4, 1.7°; 3–5, 0.5°; 3–6, −121.7°; 4–5, 121.6°; 4–6, −0.6°; 5–7, 0.1°; 5–8, −121.5°; 6–7, 122.2°; and 6–8, 0.7° (values 1–3 and 1–4 are used for L-Pro, and 2–3 and 2–4 for D-Pro).

The relationship between $^3J_{HH}$ and ϕ_{HH} was originally presented by Karplus as a "cosine squared" law (Karplus, 1959):

$$^3J_{HH} = A \cos^2 \theta_{HH} + B \quad (4)$$

and later (Karplus, 1963) as the trigonometric series

$$^3J_{HH} = A + B \cos \theta_{HH} + C \cos (2\phi_{HH}) \quad (5)$$

where A, B, and C are empirically determined parameters. Despite Karplus' caveats regarding additional factors, including substituent electronegativity (Karplus, 1963), these equations and similar variants survive no doubt due to their appealing simplicity. One popular variation (Demarco et al., 1978),

$$^3J_{HH} = A \cos^2 \theta_{HH} + B \cos \theta_{HH} + C \quad (6)$$

where A = 9.5, B = −1.6, and C = 1.8 (indicating that at the 90° minimum $^3J_{HH}$ equals 1.8 Hz) is clearly wrong for our system, as shown by a number of instances in Table 1 of very small $^3J_{HH}$ values, several within experimental error (±0.4 Hz) of zero.

Efforts to generalize the Karplus equation have led to formulations with growing numbers of empirical parameters, whose awkwardness has been justified by superior agreement with experiment. For example, in order to account properly for the electronegativies and orientations of the four substitutent groups attached to any H_A–C–C–H_B ethane fragment,

Table 5: Calculated Phase Angles, P, Pucker Angles, Φ_m, Mole Fractions, X, Spin-coupling Constants, ^3J (Hz) and Dihedral Angles, θ (deg), from Pseudorotation Analysis and Force-Field Calculations

Pro-L-boroPro

	boroPro								Pro							
	N-type			S-type			wtd. av.		N-type			S-type			wtd. av.	
P	−4.7°			167.0°					8.0°			214.3°				
Φ_m	42.8°			42.0°					48.1°			42.2°				
X	0.864			0.136					0.503			0.497				
D[b]	^3J	θ^{PR}	θ^{FF}	^3J	θ^{PR}	θ^{FF}	^3J	Δ^3J	^3J	θ^{PR}	θ^{FF}	^3J	θ^{PR}	θ^{FF}	^3J	Δ^3J
13	6.0	−38.3	−38.2	7.2	37.0		6.1	0.8	6.0	−36.3	−37.9	8.8	12.5	14.2	7.4	1.1
14	11.8	−159.5	−159.2	0.8	−84.2		103.3	0.9	10.9	−157.5	−160.2	2.4	−108.7	−106.4	6.7	0.5
35	6.1	43.2	44.7	6.6	−40.4		6.2	0.4	5.3	48.1	47.7	7.5	−34.4	−37.7	6.4	−0.7
36	1.0	−79.0	−76.3	12.4	−162.6		2.6	0.6	1.4	−74.1	−74.6	11.6	−156.6	−159.1	6.4	1.3
45	12.6	164.3	165.7	0.9	80.7		11.0	0.0	13.0	169.2	168.3	0.8	86.7	81.3	6.9	0.7
46	6.3	42.1	44.8	6.4	−41.5		6.3	−0.2	5.5	47.0	46.0	7.3	−35.5	−40.1	6.4	0.8
57	7.9	−32.3	−34.1	7.5	27.7		7.8	0.4	6.5	−42.4	−43.0	5.4	42.3	46.3	6.0	0.5
58	11.1	−153.9	−156.2	1.1	−93.9		9.7	0.4	12.3	−164.0	−166.8	0.9	−79.3	−78.0	6.6	1.4
67	0.9	89.8	86.9	10.4	149.8		2.2	0.6	0.9	79.7	79.2	12.3	164.4	167.8	6.6	1.0
68	6.9	−31.7	−35.2	8.4	98.3		7.1	0.0	5.5	−41.8	−44.5	6.5	42.9	43.5	6.0	1.0
0		42.7	40.6		−40.9					47.6	44.3		−34.9	−33.4		
1		−32.4	−30.9		27.6				−42.5	−40.6		42.2	41.3			
2		9.8	9.7		−3.7					21.1	20.5		−33.4	−33.3		
3		16.5	15.5		−21.6					8.4	7.9		11.8	11.9		
4		−36.6	−34.3		38.7					−34.6	−33.1		14.2	14.1		
ΔJ(rms) =								0.5								1.0

Pro-D-boroPro

	boroPro								Pro							
	N-type			S-type			wtd. av.		N-type			S-type			wtd. av.	
P	14.2°			165.4°					−6.2°			173.9°				
Φ_m	39.3°			38.8°					45.4°			33.4°				
X	0.272			0.728					0.524			0.476				
D[b]	^3J	θ^{PR}	θ^{FF}	^3J	θ^{PR}	θ^{FF}	^3J	Δ^3J	^3J	θ^{PR}	θ^{FF}	^3J	θ^{PR}	θ^{FF}	^3J	Δ^3J
13									5.3	−41.1	−43.5	7.8	27.2	30.5	6.5	2.2
14									11.5	−162.3	−165.8	1.0	−94.0	−90.0	6.5	0.9
23	1.4	97.8	91.9	11.6	159.0	158.7	8.9	0.6								
24	8.9	−23.4	−28.6	6.0	37.8	38.3	6.8	1.3								
35	7.2	38.6	41.5	6.8	−37.0	−41.7	6.9	−0.4	5.7	45.6	46.0	7.7	−32.7	−38.5	6.7	−1.1
36	0.8	−83.6	−79.2	12.0	−159.2	−162.0	9.0	0.4	1.2	−76.6	−75.5	11.3	−154.9	−159.1	6.0	1.9
45	1.5	159.7	162.4	0.9	84.1	79.2	3.8	0.8	12.8	166.7	167.0	0.8	88.4	80.8	7.1	0.9
46	7.2	37.5	41.7	6.8	−38.1	−41.1	6.9	−0.3	5.9	44.5	45.4	7.6	−33.8	−39.8	6.7	0.3
57	7.3	−36.3	−38.3	7.8	24.7	29.4	7.7	1.1	7.7	−33.5	−35.6	7.8	24.8	30.9	7.8	1.7
58	1.5	−157.9	−160.3	1.1	−96.9	−92.2	3.9	−0.1	11.3	−155.1	−158.6	1.3	−96.8	−91.3	6.5	0.0
67	0.8	85.8	82.7	9.6	146.8	150.0	7.2	0.0	0.9	88.6	86.0	9.9	146.9	151.5	5.2	−0.3
68	6.2	−35.7	−39.3	8.7	25.3	28.3	8.0	0.0	6.8	−32.9	−37.0	8.6	25.4	29.2	7.7	0.0
0		38.1	36.9		−37.5	−36.3				45.1	42.5		−33.2	−32.9		
1		−36.5	−34.3		24.6	24.5				−33.6	−32.6		24.8	25.4		
2		20.9	19.6		−2.3	−3.1				9.3	9.0		−6.9	−7.4		
3		2.6	3.3		−20.9	−19.4				18.6	18.2		−13.6	−13.7		
4		−25.2	−25.0		36.1	33.9				−39.4	−38.1		29.0	29.3		
ΔJ(rms) =								0.7								1.2

cyclo(Pro-L-boroPro)

	boroPro								Pro							
	N-type			S-type			wtd. av.		N-type			S-type			wtd. av.	
P	−11.9°			167.0°[a]					−15.6°			167.0°				
Φ_m	40.3°			42.0°[a]					34.9°			42.0°[a]				
X	1.000			0.000					0.930			0.070				
D[b]	^3J	θ^{PR}	θ^{FF}	^3J	θ^{PR}	θ^{FF}	^3J	Δ^3J	^3J	θ^{PR}	θ^{FF}	^3J	θ^{PR}	θ^{FF}	^3J	Δ^3J
13	5.9	−38.5	−39.7	7.2	37.0		5.9	0.0	6.5	−34.5	−42.6	7.2	37.0		6.5	1.0
14	11.8	−159.7	−160.8	0.8	−84.2		11.8	0.5	10.7	−155.7	−163.7	0.8	−84.2		10.0	1.2
35	6.7	39.9	42.2	6.6	−40.4		6.7	0.1	7.5	34.2	38.4	6.6	−40.4		7.5	0.1
36	0.9	−82.3	−78.3	12.4	−162.6		0.9	−0.9	0.8	−88.0	−82.1	12.4	−162.6		1.6	0.5
45	12.2	161.0	163.3	0.9	80.7		12.2	0.1	11.4	155.3	158.7	0.9	80.7		10.6	0.1
46	6.8	38.8	42.7	6.4	−41.5		6.8	−0.2	7.7	33.1	38.2	6.4	−41.5		7.6	0.4
57	8.5	−26.9	−29.7	7.5	27.7		8.5	0.8	9.0	−21.6	−25.1	7.5	27.7		8.9	0.4
58	10.2	−148.5	−151.7	1.1	−93.9		10.2	0.9	9.1	−143.2	−147.1	1.1	−93.9		8.6	0.6
67	1.2	95.2	91.0	10.4	149.8		1.2	−0.2	1.5	100.5	95.4	10.4	149.8		2.1	1.4
68	7.7	−26.3	−31.1	8.4	28.3		7.7	−0.7	8.6	−21.0	−26.5	8.4	28.3		8.5	−0.7
0		42.7	37.8		−40.9					33.6	33.3		−40.9			
1		−32.4	−26.3		27.6					−21.7	−21.9		27.6			
2		9.8	4.3		−3.7					1.5	1.1		−3.7			
3		16.5	19.4		−21.6					19.3	20.1		−21.6			
4		−36.6	−34.8		38.7					−32.7	−33.4		38.7			
ΔJ(rms) =								0.6								0.8

Table 5: (Continued)

	cyclo(Pro-D-boroPro)														
	boroPro							Pro							
	N-type			S-type			wtd. av.	N-type			S-type			wtd. av.	
P	10.0°[a]			168.2°				13.4°			128.7°				
Φ_m	42.0°[a]			40.6°				54.7°			60.7°				
X	0.000			1.000				0.521			0.479				
D[b]	^3J	θ^{PR}	θ^{FF}	^3J	θ^{PR}	θ^{FF}	^3J	Δ^3J	^3J	θ^{PR}	θ^{FF}	^3J	θ^{PR}	θ^{FF}	^3J	Δ^3J
13									6.1	−37.3	−39.5	3.8	56.9	46.1	5.0	0.5
14									11.1	−158.5	−162.0	2.0	−64.3	−75.7	6.8	1.5
23	1.1	93.7		11.8	160.0	162.9	8.9	0.6								
24	8.4	−27.5		5.9	38.8	41.4	6.8	1.3								
35	6.3	41.9		6.8	−39.3	−43.5	6.9	−0.4	4.4	53.7	50.5	7.0	−37.4	−36.7	5.7	2.4
36	1.0	−80.3		12.3	−161.5	−164.2	9.0	0.4	1.9	−68.5	−72.8	12.0	−159.6	−157.8	6.8	1.8
45	12.5	163.0		0.9	81.8	77.7	3.8	0.8	13.3	174.8	171.9	0.8	83.7	84.8	7.3	0.6
46	6.5	40.8		6.6	−40.4	−43.0	6.9	−0.3	4.6	52.6	48.7	6.9	−38.5	−36.2	5.7	0.0
57	7.2	−37.6		7.5	27.4	31.9	7.7	1.1	5.2	−50.4	−48.1	9.8	2.9	6.0	7.4	−0.2
58	11.8	−159.2		1.1	−94.2	−90.5	3.9	−0.1	12.8	−172.0	−172.3	4.1	−118.7	−116.2	8.7	0.7
67	0.8	84.5		10.4	149.5	152.5	7.2	0.0	1.4	71.7	75.0	5.3	125.0	127.2	3.3	0.9
68	6.2	−37.0		8.4	28.0	30.1	8.0	0.0	4.5	−49.8	−49.1	9.8	3.5	5.0	7.1	0.0
0		41.4			−40.8	−39.0				53.2	48.2		−38.0	−33.4		
1		−37.7			28.0	27.0				−50.5	−47.1		2.9	3.3		
2		19.7			−4.5	−4.4				28.5	26.9		33.3	29.9		
3		5.8			−20.7	−20.0				4.4	4.1		−56.8	−50.7		
4		−29.2			38.0	35.8				−35.6	−33.2		58.5	52.0		
ΔJ(rms) =								0.5								1.1

[a] Value fixed due to low abundance (≤15%). [b] Dihedral subscripts, two digits refer to H–C–C–H dihedrals, one digit numbers to endocyclic angles as defined with eq 1.

the following equation has been proposed (Donders, 1989):

$$^3J_{HH} = C_0 + C_1 \cos\theta_{HH} + C_2 \cos(2\theta_{HH}) + C_3 \cos(3\phi_{HH}) + S_2 \sin(2\theta_{HH}) \quad (7)$$

where

$$C_0 = 7.01 - 0.58\sum_i \lambda_i - 0.24(\lambda_1\lambda_2 + \lambda_3\lambda_4) \quad (8)$$

$$C_1 = -1.08 \quad (9)$$

$$C_2 = 6.54 - 0.82\sum_i \lambda_i + 0.20(\lambda_1\lambda_4 + \lambda_2\lambda_3) \quad (10)$$

$$C_3 = -0.49 \quad (11)$$

and

$$S_2 = 0.68\sum_i \xi_i \lambda_i^2 \quad (12)$$

Substituent orientation effects (Booth, 1965; Pachler, 1972) are accounted for by the sign factor, ξ, in eq 12, which has permissible values of +1 or −1. Group electronegativities, λ, are based on measurement of $^3J_{HH}$ in monosubstituted ethanes (Colucci et al., 1985). Cross-terms in eqs 8 and 10 account for nonadditivity of substituents when there are more than one per carbon atom. Group electronegativity values exhibit solvent effects (Colucci et al., 1986; Van Wijk et al., 1992), and most literature values were measured in $CDCl_3$. Group electronegativity values used in our pseudorotation calculations are given in Table 4. They are the most recent values for aqueous solvents supplied with PSEUROT 5.4 (Altona, 1992), supplemented by our own $^3J_{HH}$ measurements of substituted ethanes in D_2O and, in the case of -$B(OH)_2$, due to commercial unavailability of ethaneboronic acid, a value producing the best fit to our data.

A through-space effect on ^1H spin-coupling across saturated rings, the "Barfield transmission effect" (Marshall et al., 1976), is known to occur, especially in highly puckered envelope conformers, and is an option in PSEUROT. First discovered in norbornanes, the effect of orbitals from the atom at the envelope's "flap" (the C7 methylene bridge in norbornane) is known to cause as much as 3 Hz nonequivalence between *exo–exo* and *endo–endo* coupling constants (the latter being smaller) despite identical ϕ_{HH} angles. Theoretical studies on five-membered rings containing heteroatoms -N and -O (De Leeuw et al., 1983b) concluded that the Barfield effect plays an important role in proline rings, explaining inequalities in *cisoid* β-γ and γ–δ proton pairs. De Leeuw et al. found that nitrogen atoms in the bridgehead position have a smaller effect than methylene carbons, but larger than that of oxygen. A simple $\cos^2$ formula for calculating the Barfield effect was presented, supplying coefficients for bridgehead carbon and oxygen atoms, but inexplicably omitting the coefficient for nitrogen. Pseudorotation calculations in this work were carried out using a variety of coefficients for bridgehead nitrogens, yielding no improvement in fit to the data. Thus we join previous workers in not correcting for the Barfield transmission effect (De Leeuw et al., 1983a) for purely practical reasons.

Results of the pseudorotation analysis are summarized in Table 5. Convergence was obtained in all cases, with rms errors for J ranging between 0.5 and 1.2 Hz. Pucker angles average about 42° for the proline rings, in agreement with previous workers (Haasnoot et al., 1981; De Leeuw et al., 1983a), as contrasted with about 38° typical of ribose rings (Hoffman et al., 1992). Phase angles for N- and S-type species range from −16° to +14° for P_N and from 128° to 214° for P_S. When the mole fraction, X, of either N- or S-type species fell below about 15%, decreasing the reliability of the output parameters, values of Φ_m, P_N, and P_S were constrained to 42°, 10°, and 167°, respectively. The boroPro ring of open chain compounds I and II prefer the envelope conformations, probably as a result of sp^2 hybridized nitrogens, whereas the terminal proline rings, with their sp^3 hybridization, exist in twist conformations, with nearly equal N and S conformations. Compound IV shows the greatest values of pucker angle Φ_m, with 54.7° and 60.7° in the N- and S-type Pro rings, respectively, probably indicative of ring strain. The best values of the proton dihedral angles and vicinal spin coupling constants calculated

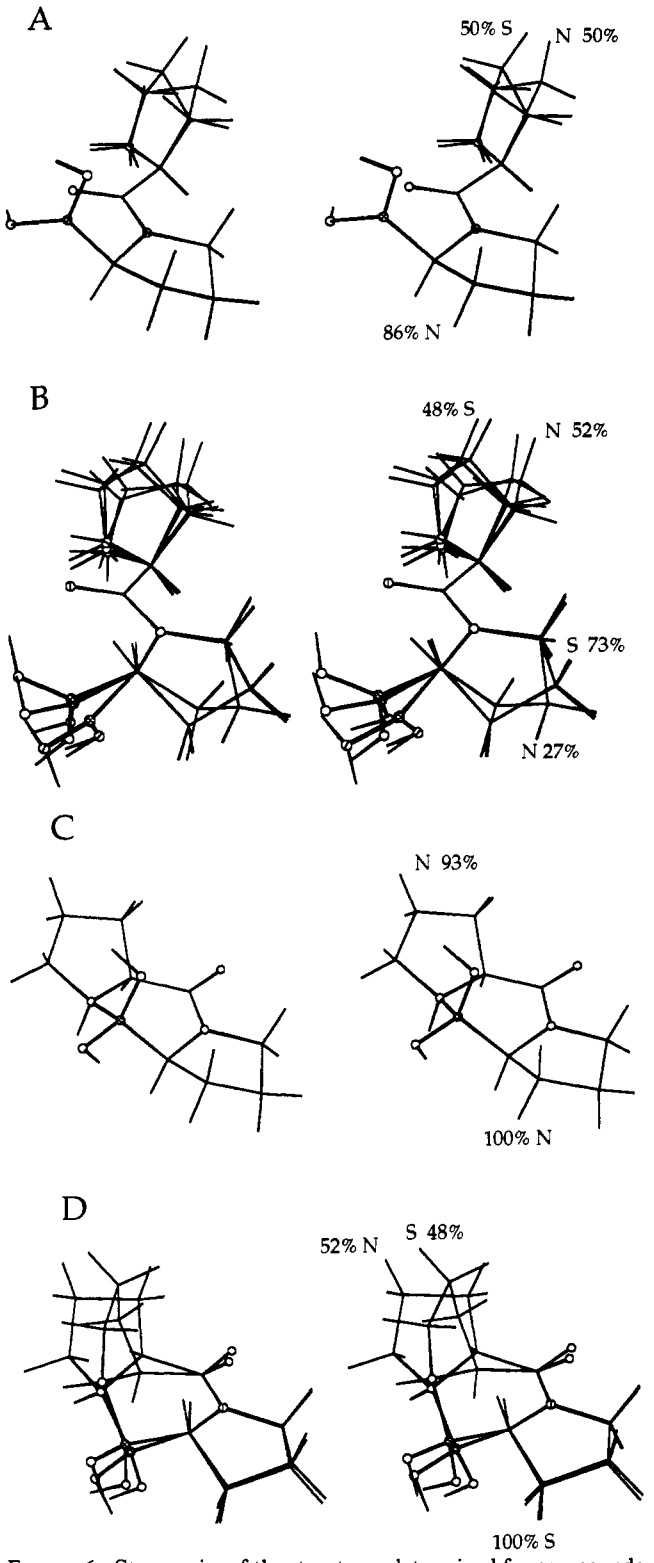

FIGURE 6: Stereopairs of the structures determined for compounds I–IV (A–D, respectively). The structures were energy-minimized via force-field calculations with endocyclic dihedral angle constraints derived from pseudorotation analysis.

by PSEUROT for N-type, S-type, and weighted averages are also listed in Table 5. From P and Φ_m, the phase and pucker angles determined by PSEUROT, the five endocyclic angles θ_0–θ_4 were calculated with eq 1 and listed in Table 5.

Computer Modeling and Force-Field Energy Minimization. Computer models of compounds I through IV were constructed and energy-minimized using QUANTA and CHARMm and are displayed as stereopairs in Figure 6.

Table 6: Peptide Dihedral Angles ψ_1 and ω_2 Calculated from CHARMm Force-Field Minimized Structures

compound	conformation	X^{PbP}	ψ_1	ω_2
Pro-L-boroPro	NN	0.503	165.9°	174.8°
	SN	0.497	168.9°	174.6°
wtd. av.			167.4 ● 2.1°	174.6 ± 0.1°
Pro-D-boroPro	NN	0.143	167.4°	−177.2°
	NS	0.381	155.3°	−175.9°
	SN	0.129	165.7°	−177.3°
	SS	0.347	158.8°	−177.6°
wtd. av.			159.6 ● 5.3°	−176.9 ± 0.9°
cyclo(Pro-L-boroPro)	NN	1.000	5.2°	−1.0°
cyclo(Pro-D-boroPro)	NS	0.521	−32.1°	7.7°
	SS	0.479	26.8°	−15.0°
wtd. av.			−3.9 ± 41.6°	−3.2 ● 16.0°

Because there is no evidence to suggest any correlation between the N ⇄ S conformational equilibria of the Pro and boroPro rings, multiple computer models having sufficient combinations of ring conformers, i.e., NN, NS, SN, and SS, were constructed in order to account for the populations determined by pseudorotation analysis. The mole fraction of each molecular conformer, e.g., NN, is the product of the populations of conformer N in the individual Pro and boroPro rings, so that

$$X_{NN}^{PbP} = X_N^{P} X_N^{bP} \tag{13}$$

and similarly for NS, SN, and SS. The contributions of molecular conformers resulting from values of X_N or X_S less than 15% was ignored.

Proper choice of the dielectric model is crucial in obtaining force-field minimizations not overwhelmed by electrostatic attractions. Good results were obtained using the distance-dependent or radial dielectric model in CHARMm (RDIE) with a value of constant EPS = 4. To include the phase and pucker angles from pseudorotation analysis, proline endocyclic angles θ_0–θ_4 were input as dihedral constraints (constraint weight = 50). Absent these constraints, CHARMm tended to underestimate pucker angles by about 8°. CHARMm parameter sets regarding boron are meager, and, except for the important B–N bond distance of 1.74 Å (Snow et al., unpublished data), default values for boron bond distances, angles, and related force constants were adopted.

Proton and endocyclic dihedral angles resulting from force-field minimizations are shown in Table 5. Good agreement is obtained between dihedral angles from pseudorotation analysis and from constrained force-field calculations, with an rms error of 3.3°, and a maximum deviation of 11.4°. Better agreement could be obtained by adding the ^{1}H dihedral angles as constraints and/or increasing all constraint weights. However, that would risk distorting carbon atom tetrahedral geometries and seems unwarranted in view of the agreement obtained by conservative measures.

With the imposition of proline conformer constraints, dihedral angles ψ_1 (N1-CA1-C1-N2) and ω_2 (CA1-C1-N2-CA2) between rings are among the few remaining degrees of freedom. Their values from the CHARMm force-field minimized structures are shown in Table 6, along with populations of various molecular conformers, weighted averages of ψ_1 and ω_2, and standard deviations of the weighted averages

$$\text{wtd. std. dev.} = \sqrt{\frac{n}{n-1}\sum X_i(\text{dev}_i)^2} \tag{14}$$

where n is the total number of observations. As shown in Table 6, when boroPro has the N conformation, ψ_1 is in the

Table 7: Comparison of Average Interproton Distances (Å) of Pro-L-boroPro in D_2O at pH = 2 Calculated by Two Methods: NOESY Cross-Peak Volumes with Two-Proton Assumption vs Pseudorotation Analysis and Force-Field Calculations

assignment	label[a]	NOESY distance[b]	PR/FF Distance[c]	dev.
bP:A/bP:2B	10	2.37 ± 0.14	2.44 ± 0.00	0.07
bP:A/bP:1B	12	3.12 ± 0.21	3.06 ± 0.00	–0.06
bP:A/bP:2G	11	2.86 ± 0.18	2.77 ± 0.00	–0.09
bP:A/bP:2D	5	3.38 ± 0.30	3.59 ± 0.00	0.21
bP:1B/bP:2B		1.81 ± 0.01	1.77 ± 0.00	–0.04
bP:1B/bP:2G		2.89 ± 0.15	3.05 ± 0.00	0.16
bP:1B/bP:1D	9	2.86 ± 0.01	2.81 ± 0.01	–0.05
bP:2G/bP:2D	7	2.42 ± 0.01	2.38 ± 0.00	–0.04
bP:1G/bP:2D		2.83 ± 0.06	2.73 ± 0.00	–0.10
bP:2D/bP:1D		1.78[d]	1.78 ± 0.00	0.00
bP:2D/P:A	1	2.33 ± 0.21	2.23 ± 0.01	–0.10
bP:2D/P:2B	6	3.36 ± 0.06	3.27 ± 0.21	–0.09
bP:1D/P:A	2	2.73 ± 0.07	2.92 ± 0.01	0.19
bP:1D/P:2B	8	2.57 ± 0.00	2.55 ± 0.45	–0.02
P:A/P:2B	3	2.57 ± 0.21	2.38 ± 0.09	–0.19
dev. (rms) =				0.12

[a] Corresponding to Figures 2C and 3. [b] Averages and standard deviations derived from cross-peak volumes on opposite sides of the diagonal. [c] Weighted averages and weighted standard deviations (eq 14) from multiple structures. [d] Geminal H–H distance taken from the computer model as a reference.

165–167° range, but when it has the S conformation, ψ_1 is in the 155–159° range, the N vs S difference indicating some steric interaction between rings. Because of peptide C–N double bond character, ω_2 deviates little from the expected value of 180° in the *trans*, open-chain compounds I and II, or from the expected 0° in the *cis*, cyclic compounds, III and IV.

Comparison of Distances from NOESY vs Force-Field Calculations. In many studies of solution structures, NOESY, the 2D NMR spectroscopic method which responds to through-space internuclear interactions, is the method of choice for determination of ^1H–^1H distances. In addition to poor inherent sensitivity, however, NOESY suffers a number of limitations. Small cross-peaks are associated with greater relative error, so that the most valuable (i.e., large) distances are invariably the most uncertain. To minimize systematic errors due to spin diffusion at long mixing times, NOESY spectra are normally acquired with reduced mixing times, corresponding to early-stage NOE buildup. However, this tends to increase the contributions of random errors and other systematic errors, such as incompletely cancelled through-bond COSY peaks (e.g., peak 4 in Figure 2C).

When spatial averaging occurs among significant conformer populations, as in the present study, utilization of NOESY data in any quantitative sense is at its most doubtful (Neuhaus & Williamson, 1989). Theory has been established for "uniform averaging", where nuclei range with equal probabilities within certain distance boundaries (Braun et al., 1981). Such distance averaging is nonlinear, depending upon r^{-3} for averaging, which is rapid compared to molecular tumbling rates, and upon r^{-6} for slow averaging. The theory, however, is inapplicable to the present case, where intramolecular distances vary among discrete values. Regardless how distances would be averaged in this situation, the populations of contributing species are clearly indeterminate.

Limitations notwithstanding, NOESY spectra play essential roles in the present study for assignment of ^1H resonances and for evaluating the outcome of force-field minimizations. A mixing time of 600 ms was chosen for the four compounds based on determination of ~800 ms as the time of maximum NOE buildup for one of the compounds. NOESY cross-peak volumes were measured and subjected to first-order analysis using a two-proton model, i.e., assuming each pair to interact independently of all other protons. Cross-peak volumes in this model are proportional to r^{-6}, and with referencing vs the large cross-peaks from geminal protons of known separation (1.78 Å), average NOESY distances were calculated, as shown in Table 7. Only cases giving unambiguously assignable pairs of cross-peaks on both sides of the diagonal were included. These distances are compared with *linear* weighted average distances (and weighted standard deviations according to eq 14) obtained from the energy-minimized structures.

As shown in Table 7, the agreement between the distances from NOESY spectra and from the computer models is very good for compound I, producing an rms error of ±0.12 Å. The agreement is thought to be fortuitous, however, because, for compounds II–IV, higher errors are obtained. T_1 values of the ^1H atoms in Pro-D-boroPro were measured, ranging from 0.5 to 2.0 s. Increasing the relaxation delay from 1.3 to 5.0 s surprisingly did not improve the fit of NOESY to computer model distances. The agreement resulting from NOESY distances is not bad in light of the simplifying assumptions, and specific assignment clues provided by NOESY spectra are invaluable in determining the structures shown in Figure 6.

ACKNOWLEDGMENT

We are grateful to Dr. Clemens G. Anklin of Bruker Instruments, Billerica, MA, for running the 600-MHz ^1H 1D NMR spectra. We acknowledge helpful discussions with Prof. Michael Barfield, and we thank Prof. Cornelis Altona for providing source code of PSEUROT 5.4 and helpful advice on its application.

REFERENCES

Altona, C. (1992) University of Leiden, Leiden, The Netherlands.
Altona, C., & Sundaralingam, M. (1972) *J. Am. Chem. Soc. 94*, 8205–8212.
Altona, C., Ippel, J. H., Westra Hoekzema, A. J. A., Erkelens, C., Groesbeek, M., & Donders, L. A. (1989) *Magn. Reson. Chem. 27*, 564–576.
Ansorge, S., & Ekkehard, S. (1987) *Acta Histochem. 82*, 41–46.
Attimonelli, M., & Sciacovelli, O. (1980) *Org. Magn. Reson. 13*, 277–278.
Bachovchin, W. W., Plaut, A. G., Flentke, G. R., Lynch, M., & Kettner, C. A. (1990) *J. Biol. Chem. 265*, 3738–3743.
Bendall, M. R., & Pegg, D. T. (1983) *J. Magn. Reson. 53*, 144–148.
Booth, H. (1965) *Tetrahedron Lett.*, 411–416.
Bothner-by, A. A., & Castellano, M. S. (1968) in *Computer Programs for Chemistry* (DeTar, D. F., Ed.) Vol. 1, Chapter 3, Benjamin, New York.
Braun, W., Bösch, C., Brown, L. R., Go, N., & Wüthrich, K. (1981) *Biochim. Biophys. Acta 667*, 377–396.
Braunschweiler, L., & Ernst, R. R. (1983) *J. Magn. Reson. 53*, 521–528.
Brooks, B. R., Bruccoleri, R. E., Olafson, B. D., States, D. J., Swaminathan, S., & Karplus, M. (1983) *J. Comput. Chem. 4*, 187–217.
Callebaut, C., Krust, B., Jacotot, E., & Hovanessian, A. G. (1993) *Science 262*, 2045–2050.
Campbell, I. D., Dobson, C. M., Williams, R. J. P., & Xavier, A. V. (1973) *J. Magn. Reson. 11*, 172–181.
Campbell, I. D., Dobson, C. M., Jeminet, G., & Williams, R. J. P. (1974) *FEBS Lett. 49*, 115–119.
Cavanagh, J., & Rance, M. (1992) *J. Magn. Reson. 96*, 670–678.

Clore, G. M., Kimber, B. J., & Gronenborn, A. M. (1983) *J. Magn. Reson. 54*, 170–173.
Colucci, W. J., Jungk, S. J., & Gandour, R. D. (1985) *Magn. Reson. Chem. 23*, 335–343.
Colucci, W. J., Gandour, R. D., & Mooberry, E. A. (1986) *J. Am. Chem. Soc. 108*, 7141–7147.
De Leeuw, F. A. A. M., & Altona, C. (1983) *J. Comput. Chem. 4*, 428–437.
De Leeuw, F. A. A. M., Altona, C., Kessler, H., Bermel, W., Friedrich, A., Krack, G., & Hull, W. E. (1983a) *J. Am. Chem. Soc. 105*, 2237–2246.
DeLeeuw, F. A. A. M., Van Beuzekom, A. A., & Altona, C. (1983b) *J. Comput. Chem. 4*, 438–448.
Demarco, A., Llinas, M., & Wüthrich, K. (1978) *Biopolymers 17*, 617–636.
Derome, A. E. (1990) *J. Magn. Reson. 88*, 177–185.
Donders, L. A. (1989) Ph.D. Thesis, University of Leiden, Leiden, The Netherlands.
Eliel, E. L., Allinger, N. L., Angyal, S. J., & Morrison, G. A. (1965) *Conformational Analysis*, pp 200–206, Wiley, New York.
Ferrige, A. G., & Lindon, J. C. (1978) *J. Magn. Reson.* 31, 337–340.
Flentke, G. R., Munoz, E., Huber, B. T., Plaut, A. G., Kettner, C. A., & Bachovchin, W. W. (1991) *Proc. Natl. Acad. Sci. U.S.A. 88*, 1556–1559.
Frohman, L. A., Downs, T. R., Heimer, E. P., & Felix, A. M. (1989) *J. Clin. Invest. 83*, 1533–1540.
Gutheil, W. G., & Bachovchin, W. W. (1993) *Biochemistry 32*, 8723–8931.
Haasnoot, C. A. G., De Leeuw, F. A. A. M., De Leeuw, H. P. M., & Altona, C. (1981) *Biopolymers 20*, 1211–1245.
Hafler, D. A., Fox, D. A., Benjamin, D., & Weiner, H. L. (1986) *J. Immunol. 125*, 42–57.
Hafler, D. A., Chofflon, M., Benjamin, D., Dang, N. H., & Breitmeyer, J. (1989) *J. Immunol. 142*, 2590–2596.
Hanski, C., Huhle, T., & Reutter, W. (1985) *Biol. Chem. Hoppe-Seyler 366*, 1169–1176.
Hanski, C., Huhle, T., Gossrau, R., & Reutter, W. (1988) *Exp. Cell Res. 178*, 64–72.
Hoffman, R. A., Van Wijk, J., Leeflang, B. R., Kamerling, J. P., Altona, C., & Vliegenthart, J. F. G. (1992) *J. Am. Chem. Soc. 114*, 3710–3714.
Karplus, M. (1959) *J. Chem. Phys. 30*, 11–15.
Karplus, M. (1963) *J. Am. Chem. Soc. 85*, 2870–2871.
Kelly, T. A., Fuchs, V. U., Perry, C. W., & Snow, R. J. (1993a) *Tetrahedron 49*, 1009–1016.
Kelly, T. A., Adams, J., Bachovchin, W. W., Barton, R. W., Campbell, S. J., Coutts, S. J., Kennedy, C. A., & Snow, R. J. (1993b) *J. Am. Chem. Soc. 115*, 12637–12638.
Kidd, R. G. (1983) in *NMR of Newly Accessible Nuclei* (Lazlo, P., Ed.) Vol. 2, pp 49–77, Academic, New York.
Kubota, T., Flentke, G. R., Bachovchin, W. W., & Stollar, B. D. (1992) *Clin. Exp. Immunol. 89*, 192–197.
Kumar, A., Ernst, R. R., & Wüthrich, K. (1980) *Biochem. Biophys. Res. Commun. 95*, 1–6.
Marion, D., & Wüthrich, K. (1983) *Biochem. Biophys. Res. Commun. 113*, 967–974.
Marshall, J. L., Walter, S. R., Barfield, M., & Segre, A. L. (1976) *Tetrahedron 32*, 537–542.
Miyamoto, Y., Ganapathy, V., Barlas, A., Neuber, K., Barth, A., & Leibach, F. H. (1987) *Am. J. Physiol. 252*, F670–F677.
Miyamoto, Y., Ganapathy, V., & Leibach, F. H. (1988) *Contrib. Nephrol. 68*, 1–5.
Momany, F., & Rone, R. (1992) *J. Comput. Chem. 13*, 888–900.
Neuhaus, D., & Williamson, M. P. (1989) *The Nuclear Overhauser Effect in Structural and Conformational Analysis*, pp 170–174, VCH Publishers, New York.
Pachler, K. G. R. (1972) *J. Chem. Soc., Perkin Trans. II*, 1936–1940.
Pogliani, L., Ellenberger, M., & Valat, J. (1975) *Org. Magn. Reson. 7*, 61–71.
Putochin, N. (1926) *Chem. Ber. 59*, 1987–1998.
Rance, M., Sørensen, O. W., Bodenhausen, G., Wagner, G., Ernst, R. R., & Wüthrich, K. (1983) *Biochem. Biophys. Res. Commun. 117*, 479–485.
Schön, E., & Ansorge, S. (1990) *Biol. Chem. Hoppe-Seyler* 371, 699–705.
Schön, E., Mansfeld, H. W., Demuth, H. U., Barth, A., & Ansorge, S. (1985) *Biomed. Biochim. Acta 44*, K9–K15.
Schön, E., Jahn, E., Kiessig, S. T., Demuth, H. U., Neubert, K., Barth, A., Von, B. R., & Ansorge, S. (1987) *Eur. J. Immunol. 17*, 1821–1826.
Schön, E., Demuth, H. U., Eichmann, E., Horst, H. J., Korner, I. J., Kopp, J., Mattern, T., Neubert, K., Noll, F., Ulmer, A. J., Barth, A., & Ansorge, S. (1989) *Scand. J. Immunol. 29*, 127–132.
Shaka, A. J., Lee, C. J., & Pines, A. (1988) *J. Magn. Reson. 77*, 274–293.
Tsilikounas, E., Kettner, C. A., & Bachovchin, W. W. (1993) *Biochemistry 32*, 12651–12655.
Van Wijk, J., Huckriede, B. D., Ippel, J. H., & Altona, C. (1992) *Methods Enzymol. 211*, 286–306.